Geoscience Letters

RESEARCH LETTER

Open Access

Sensor orientation of the TMD seismic network (Thailand) from P-wave particle motions

Patinya Pornsopin[1,2], Passakorn Pananont[2*], Kevin P. Furlong[3] and Eric Sandvol[4]

Abstract

The Thai Meteorological Department (TMD) seismic network began development in 2008. There are a total of 71 seismic stations consisting of 26 borehole stations and 45 surface stations currently installed. The three-component data from the TMD seismic network have been widely used in previous seismological studies. In a recent analysis, we have found that sensor orientation as reported in the site metadata is sometimes significantly incorrect, especially for borehole stations. In this study, we analyze P-wave polarization data from regional and teleseismic earthquakes recorded in the network to estimate the true instrument orientation relative to geographic north and compare that to station metadata. Of the 45 surface stations, we found that at present, ~ 82% are well oriented (i.e., aligned within 0–15° of true north). However, 8 sites have sensors misoriented by more than 15°, and some stations had a temporal change in sensor orientation during an upgrade to the seismic system with replacement of the sensor. We also evaluated sensor orientations for 26 TMD borehole seismic stations, from 2018 to the 2022. For many of the borehole stations, the actual sensor orientation differs significantly from the TMD metadata, especially at short-period stations. Many of those stations have sensor misorientations approaching 180°, due to errors in the ambient noise analysis calibration techniques used during installation. We have also investigated how this sensor misorientation affects previous seismic studies, such as regional moment tensor inversion of earthquakes sources and receiver function stacking. We have found that the large deviations in sensor orientation can result in erroneous results and/or large measurement errors. A cause of the orientation error for borehole sites could be a combination of strong background surface ambient seismic noise coupled with an incorrect reference instrument response.

Keywords Sensor orientation, Seismic network, Earthquake, Thailand

Introduction

Network seismic stations typically use a three-component sensor (2 horizontal, 1 vertical) with each component mutually perpendicular. For stations in the Thai Meteorological Department (TMD) network the normal seismometer orientation is for one horizontal component to be aligned north–south and the other east–west, which is set during installation. For borehole seismometers it is difficult to control the orientation of the horizontal components during installation, but knowing the actual orientations allows the data to be rotated into a N/S–E/W framework before analysis of the waveform data.

*Correspondence:
Passakorn Pananont
fscipkp@ku.ac.th
[1] Earthquake Observation Division, Thai Meteorological Department, Bangkok, Thailand
[2] Department of Earth Sciences, Faculty of Science, Kasetsart University, Bangkok, Thailand
[3] Department of Geosciences, The Pennsylvania State University, University Park, Pennsylvania, USA
[4] Department of Geological Sciences, University of Missouri, Columbia, Missouri, USA

Misorientation of a seismometer at a surface site can occur during installation for a variety of reasons such as a magnetic compass affected by site-specific variations, or a magnetic deviation caused by nearby magnetic field sources or interference. The GSN (Global Seismographic Network) stopped using magnetic methods in 2009, because of the potential for large sensor orientation errors (Ringler et al. 2013). Recently, Wang et al. (2016) analyzed sensor orientation for the NorthEast China Seismic Array using P-wave particle motions of earthquakes at distances of 5°–90°. Using this methodology, they determined orientation results consistent with gyrocompass measurements. Scholz et al. (2017) estimated the orientation of ocean-bottom seismometers in the RHUM-RUM experiment using P-wave and Rayleigh wave polarizations. Their results show good agreement in orientation using these two methods, with have an average uncertainty of 11° (P-wave) and 16° (Rayleigh wave) per station. Ensing and van Wijk (2018) used cross correlation of Rayleigh wave ambient seismic noise to estimate the borehole and surface station orientation of stations in the Auckland volcanic field in New Zealand. They found an average standard deviation orientation misfit across the network to be 11°, with the orientations agreeing with results from the P-wave polarization technique. Ojo et al. (2019) estimated sensor misorientation of 1075 broadband seismic stations in Africa using three independent methods consisting of P-wave particle motion, P-wave energy on the transverse component and Rayleigh wave arrival angles from teleseismic earthquakes, and found that ~ 35% of stations were well oriented (within 3°) and ~ 17% of the stations are misaligned by more than 10°. Braunmiller et al. (2020) obtained sensor orientations for the Iranian National Seismic Network (INSN) of the Iranian Seismological Center (IRSC) by using P-wave particle motion. More than 50% of all stations are oriented within 15° of true north. Büyükakpınar et al. (2021) assessed the orientation of the horizontal components of the 123 broadband stations of the KOERI Seismic Network (Turkey) based on the polarization of P waves and Rayleigh waves, obtaining consistent results from both methods.

The Thai Meteorological Department (TMD) is the principal Thailand agency that locates and catalogs earthquakes that occur in Thailand and in nearby regions. TMD began development and installation of their seismic network in 2008, which initially consisted of 8 intermediate-period (Nanometrics Trillium-40) and 7 broadband (Nanometrics Trillium-120P) seismic stations (Phase I). In 2010 (Phase II), TMD added 15 short-period (Geotech S-13) and 10 broadband (Geotech KS-2000) seismic stations and 1 borehole broadband (Geotech KS-2000BH) at the TMD facility in Bangkok. For the purpose of increasing the earthquake detection capability of the TMD seismic network, an additional 15 short-period (Guralp CMG-3TB-1 s) and 10 broadband (Guralp CMG-3TB-120 s) borehole stations (at a depth of 30 m) including 5 broadband surface stations (Guralp CMG-3T-120 s) were installed during 2018 (Phase III). At this time 6 stations (CMAI, KHLT, LAMP, MHMT, PANO and RNTT) of Phase I and Phase II were upgraded to 2 short-period (Guralp CMG-3ESP-1 s) and 4 broadband (Guralp CMG-3T-120 s) seismic stations. Phase I and Phase II of the TMD seismic network were in continuous operation until the end of 2020, when TMD replaced the instruments at all stations with Guralp equipment including 19 short-period (Guralp CMG-3ESP-1s) and 15 broadband seismometers (Guralp CMG-3T-120 s). TMD shares the real-time data from 18 broadband seismic stations with the Incorporated Institutions for Seismology (IRIS) Data Management Center (DMC) for which the FDSN code is "TM". These data have been widely used by many researchers for over ten years.

The TMD regional seismic network currently has a total of 71 broadband and short period seismic stations consisting of 45 surface stations (station details are shown in Additional file 1: Table S1) and 26 borehole stations (station details are shown in Additional file 1: Table S2). The distribution of TMD seismic stations across Thailand is shown in Fig. 1. During seismometer installation, TMD identified true north for surface stations using a compass and transferring a reference line to the sensor platform. The instrument was then rotated to align with the reference line. To identify true north for borehole stations, TMD used a comparison of ambient noise cross-correlation at a nearby surface seismometer with borehole seismometer.

In this study, we have estimated sensor misorientations from true north for the 71 stations of TMD seismic network using P-wave polarizations from regional and teleseismic earthquakes (Braunmiller et al. 2020). Additionally, in order to investigate how these station misorientations may affect various seismological analyses, we also explore the effects of misorientation on the moment tensor inversions of earthquakes to compare with focal mechanism results obtained before and after correcting station orientation. We also evaluate the effects on receiver function stacking results at borehole stations that have large orientation differences between what is in the original metadata and after correcting the alignments.

Orientation analysis and results

To determine the correct (true north) orientation for a seismic sensor, we have used an analysis of the P-wave particle motions of regional and teleseismic earthquakes.

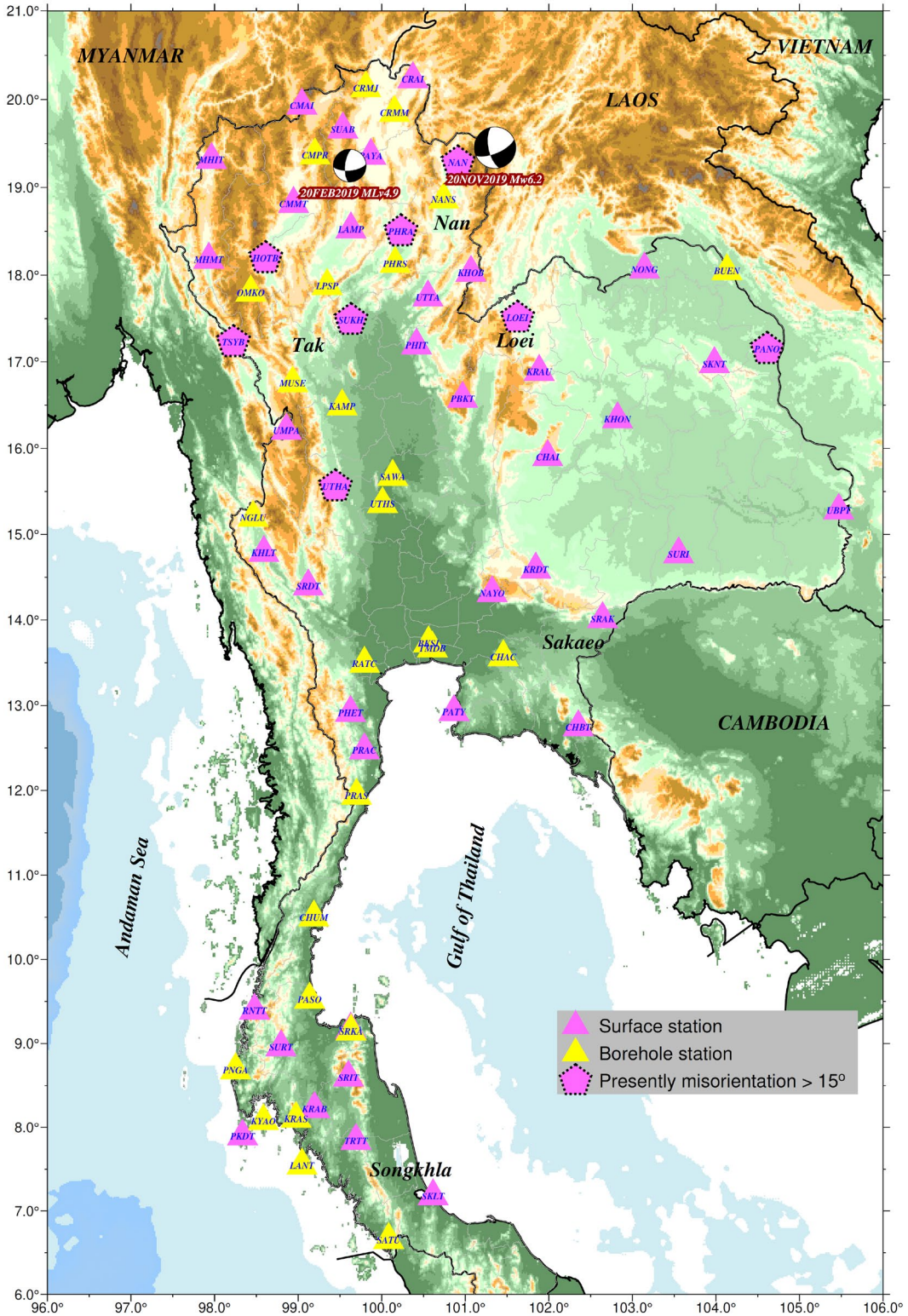

Fig. 1 Topographic map showing the locations of the 71 TMD seismic stations used in this study. The pink triangles are the 45 surface seismometers and the yellow triangles are the 26 borehole seismometers. The focal mechanisms shown are for the two earthquakes (magnitude 6.2 Mw located in Laos and MLv 4.9 in Wang Nuea, Lampang province) analyzed in the RMT inversion after correction of sensor orientation

This is a simple method that assumes a homogeneous and isotropic medium beneath the station. The vertical and horizontal (Z, N and E) components of the seismic signal are rotated into the vertical, radial, and transverse (Z, R and T) coordinates based on the earthquake to station ray path. The P-wave particle motion or energy should be large on the vertical and radial components and minimal on the transverse component for an ideal Earth. The rotation of the Z, N, E signal components is varied to achieve the effect of minimizing the transverse component. We use a large number of earthquakes from different back-azimuths to reduce any effects from local structure and anisotropy beneath the station, and perform a systematic search through rotations from 0° to 180° to find a best-fit station orientation (Niu & Li 2011; Wang et al. 2016). We also follow the approach of Braunmiller et al. (2020) by adding additional quality controls to eliminate effects of component malfunction or missing horizontal components for automatic processing. These include signal strength, similarity of vertical and radial components and transverse-to-radial energy ratio.

We collect a 60-s segment of raw waveform data around the predicted P-wave arrival from earthquakes at distances between 5 and 100 degrees (based on the USGS earthquake catalog), with minimum earthquake magnitudes of 5.9, and then we select a 12-s time window for P-wave particle motions analysis extending from − 3 s before to 9 s after the predicted P-wave arrival; windowing the data in this way helps to reduce P-wave coda contamination. All waveform data were filtered using a bandpass filter of 0.02–0.2 Hz (5–50 s), the same frequency range used by Niu and Li (2011), Ojo et al. (2019) and Zeng et al. (2020) for sensor orientation analysis from P-wave particle motion. Earthquakes during 2018 to 2022 (~ 300 events for each station) for stations installed after 2017 and earthquakes between 2009 and 2017 (more than 500 events for each station) for stations installed before 2017 are used in this analysis minimizing the P-wave or PP-wave energy on the transverse component to estimate the station orientation in terms of the azimuth of north component (i.e., the HHN, EHN, BHN, CHN, SHN channels at TMD stations). We consider the quality of orientation results to get a robust final estimate from (1) a threshold for the cross-correlation between vertical and radial components of > 0.45; (2) a threshold for signal-to-noise ratio on vertical component of > 4.5 dB which is defined as the ratio of root mean square (RMS) level of the signal and noise in the same time window as P-wave particle motions analysis; (3) a threshold for the transverse-to-radial ratio (1—T/R) of > 0.45, and (4) a threshold for the radial-to-vertical ratio (1—R/Z) of > − 1. We estimate the (correct) final azimuth and uncertainty by removing outliers based on the median absolute deviation (MAD) method, with a threshold for inclusion of lower than 5 MAD (Doran & Laske 2017). We then calculate the directional mean value using a bootstrap method of random sampling with replacement from 5000 bootstrap iterations. The 95% confidence interval of the circular mean is given as the uncertainty of estimation. We also use the kernel density estimation (KDE) at 95% confidence interval to create a smooth curve (KDE plot) of orientation data. This is to help visualize the potential non-unimodality case (Weglarczyk 2018).

We found that sensor orientations for 45 TMD surface seismic stations (Additional file 1: Table S1), are within 15° from true north (82% of all TMD surface stations presently). For example, Fig. 2a shows the orientation result and quality control of the LAMP (2018–2022) station that is clearly aligned with north (using 562 events, with 423 events passing quality control). Some sites have sensors misoriented more than 15° including HOTB, LOEI, NAN (during 2020–2022), PANO (during 2018–2022), PHRA, SRIT (during 2009–2017), SUKH (during 2020–2022), TSYB, UBPT (during 2009–2017), UMPA (during 2009–2013) and UTHA (during 2020–2022). We found that from 2009 to 2014, the PHRA station had the largest misorientation of about 154° (e.g., the orientation result shown in Fig. 2b), oriented counterclockwise from true north. After 2014, the orientation was changed to a misorientation of 12° after manual adjustment. However, when the sensor was replaced in 2020, the misorientation become 157°. We also found that the UMPA station had a significant misorientation of − 34° between 2009 to 2013, but after 2014 the orientation returned to true north after TMD replaced the sensor in response to a component malfunction. Significantly large misorientation errors of more than ± 20° were found at stations KRAB, PANO (during 2009–2017) and SURA. These stations have a very low number of earthquake events that passed quality control, likely indicating that some sensor components malfunctioned or failed (which is found in an examination of the raw data).

We also evaluated the sensor orientations for the 26 TMD borehole seismic stations for the time period from 2018 to 2022 (Additional file 1: Table S2). Our results show average orientation errors about ± 15°. Figure 3a shows the orientation result and quality control of CRMM (2018–2022) station that the orientation is rotated 140.3° clockwise from true north (using 535 events, with 274 events passing quality control). When borehole instruments are installed, one cannot control or specify the orientation (it can rotate on installation), and therefore all borehole instruments require post-installation analyses to determine their actual orientation. Although the average misorientation for these stations is relatively small, we have found that

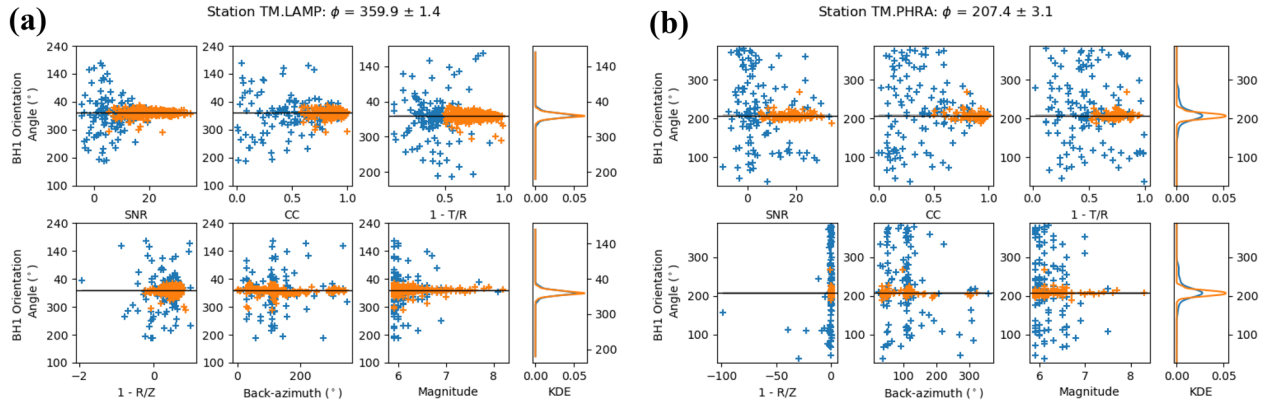

Fig. 2 Orientation results and quality control for **a** LAMP (2018–2022) and **b** PHRA (2009–2014) surface seismic stations. Results at LAMP, which include 562 events analyzed (+blue) and the 423 events (+orange) that passed quality control, shows that for high-quality events the sensor appears to be aligned with north (359.9° ± 1.4°). Results at PHRA which include 213 analyzed teleseismic events (+blue) and the 84 events (+orange) that passed quality control, show that for high-quality events the orientation of seismometer component (BHN) is rotated 207.4° ± 3.1° clockwise from true north

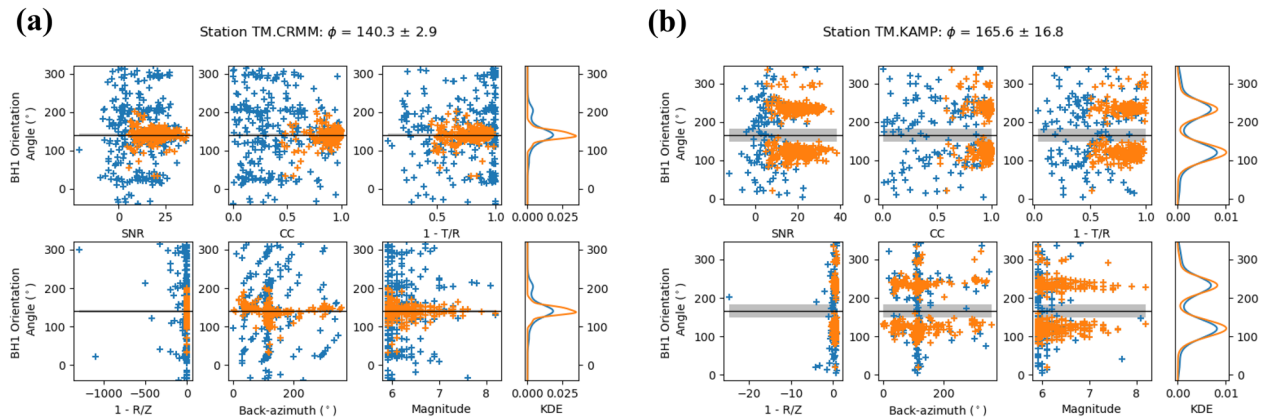

Fig. 3 Orientation and quality control for **a** CRMM (2018–2022) borehole seismic station shows that the orientation of the seismometer component (HHN) is rotated 140.3° ± 2.9° clockwise from true north with differences from the initial TMD (metadata) orientation of 114° clockwise. At CRMM, 535 events (+blue) were analyzed and 274 events (+orange) passed quality control; and **b** the KAMP borehole seismic station shows a temporal change in sensor orientation. Of the 548 events analyzed (+blue) 420 events (+orange) passed quality control. During the 2018–2022 period two orientations were found for these data at ~ 237° and ~ 126°

most of the borehole stations (80% of all TMD borehole stations) had large orientation result differences from the initial TMD (metadata) orientation. This is especially the case for the short period borehole stations, which have orientation differences from TMD metadata approaching 180°. We also have found that stations BUEN, CHUM, KAMP and LPSP had temporal changes in sensor orientation in the time period. Figure 3b shows temporal changes in sensor orientation of KAMP station of ~ 237° and ~ 126° during 2018–2022. This is a result of instrument replacements on 4 July 2020, causing changes in instrument orientation.

At initial installation, TMD stations are orientated with the use of a standard magnetic compass. This can have deviations larger than 5° from the true north, even in the case of no magnetic disturbances in the nearby surroundings (Vecsey et al. 2017). TMD determined borehole seismometer orientations during installation by placing a surface seismometer on the ground nearby and comparing the signals (ambient vibration) between the surface and borehole seismometer (30 m. deep). Errors in orientation may occur from (1) the assumed orientation of the reference surface sensor is not correct; (2) extraneous, transient vibrations near the station such as cars,

footsteps, construction machines, wind, etc., disturb the results; and (3) a significant difference in seismometer response between the reference surface sensor and borehole seismometer.

Borehole sensor orientation of TMD

To identify possible causes for the very large differences between final (correct) orientation and the initial TMD (original metadata) orientation at some TMD borehole stations, and some stations have a discrepancy close to 180° such as CHUM, CMPR, KAMP, KRAS, KYAO, LPSP, NANS, OMKO, PHRS, SATU and UTHS, we tested the potential that local environmental seismic noise at the time of calibration could produce an incorrect relative orientation at the TMDB borehole station, located in Bangna, Bangkok. The TMD installed new equipment, a Guralp CMG-3TB 120 s (calibrated orientation) with Affinity digitizer at the beginning of 2021 and as noted in Additional file 1: Table S2, this station has the correct orientation. First, we compared the orientation results obtained for differences in seismic noise between day and night times for the TMDB station. We used a broadband sensor, a Guralp CMG-3T 120 s and Affinity digitizer, as the reference (surface) sensor, which has the same instrument response and sampling rate (100sps) as the TMDB. We installed this reference surface sensor on the concrete base around the top of the borehole. We tested the effect of daytime and nighttime noise by choosing data for analyzing during 05:00–06:00 UTC and 18:00–19:00 UTC (12:00–13:00 and 01:00–02:00 local time, respectively). Then the recorded N/S component data from the reference sensor were correlated with N/S and E/W components of TMDB using the Blacknest correlation method (Burch & Atomic Weapons Research Establishment (Great Britain), 1993). For the daytime data, the results show that the N/S component of TMDB borehole sensor was − 3.9° off from the true north, this is seen as a peak coherence curve as ~ 0.65 (Additional file 1: Fig. S1a and S1b). For the nighttime data, the result shows a good coherence of 0.85 at -0.6° angle of rotation (Additional file 1: Fig. S1d and S1e). The nighttime data analysis also shows a smoother coherence curve at frequencies between 0.1 and 0.7 Hz (Additional file 1: Fig. S1f). A power spectrum density (PSD) of environmental ground motion noise during the daytime is about 10-20 dB more than that of nighttime, for data in the frequency band ranging from 0.1–0.25 Hz. The high background noise during the daytime could cause sensor orientation analysis results to differ by ~ 3° between daytime and nighttime.

We also experimented with how differences between the instrument response of the reference and test sensors could affect the orientation result by using a short period Guralp CMG-3ESPC 1 s + Affinity digitizer as a reference correlation with the TMDB broadband down-hole sensor, Guralp CMG-3 TB (120 s). We found that with the test sensor aligned 178° from true north, we obtained a high coherence of ~ 0.8 (Additional file 1: Fig. S2); that is, the orientation is almost reversed. This is a result of a difference in instrument response, with the phase response of a Guralp CMG-3ESPC (1 s) different from a Guralp CMG-3 TB (120 s) by ~ 180° in the frequency range ~ 0.1–0.4 Hz (Additional file 1: Fig. S3). In addition, we found that the instrument response of the Guralp CMG-3ESPC (1 s) sensor has a 150–180 degrees phase difference from 0.005 to 0.5 Hz. Therefore, it is important to know the instrument responses of the sensors before conducting the orientation analysis.

Discussion

To explore the effects these instrument misorientations may have had on previous seismological analyses, we conducted a qualitative reliability examination of the result. We examined the seismograms (radial and tangential) from a large regional event using the original incorrect orientations and the correct orientations at the RATC station. RATC had a difference in orientation before and after correction of 84°. We use the M 6.5 Taiwan earthquake, which occurred on 17 September 2022, (back-azimuth of 62° and distance of 22.6° from the RATC station) for this test. The transverse component using the incorrect orientation shows very high amplitude of P-wave, which is not correct, as it should have the least energy on P-wave on the transverse component. After correcting the orientation (322° from north), the transverse component shows very low energy while the radial component shows very high energy (Additional file 1: Fig. S4). This observation indicates that our orientation result is reasonable. This orientation correction is also supported by the misorientation values estimated by analyzing P-wave particle motion, which are consistent with the gyrocompass measurements (Wang et al. 2016).

In addition, we have compared the impact of the change in orientation on regional moment tensor and receiver function analyses for specific events obtained using both orientations. We conducted regional moment tensor (RMT) inversions (Herrmann 2013) for earthquakes located in the Laos–Thailand border area, where a M_w 6.2 (USGS) occurred at 23:50:43 on 20 November 2019 (19.453°N 101.356°E) and the Wang Nuea, Lampang, Thailand (19.249°N 99.617°E) earthquake at 2019-02-20 09:05:41 with magnitude MLv 4.9. We used these RMT results to compare with focal mechanism results determined before (from TMD metadata) and after correcting for the correct orientation of these stations. We also analyzed receiver function stacking results at several

borehole stations that have large differences between original orientations (metadata) and after corrections.

Regional moment tensor (RMT) solutions

We compared RMT inversion results for a strong earthquake that occurred in the border area between northern Thailand (Nan province) and Laos (19.453°N 101.356°E) on 2019-11-20 23:50:43. It caused damage and was felt in Laos and Thailand. It has a USGS reported magnitude of $6.2M_{ww}$ at 10 km depth, with a USGS w-phase moment tensor indicating oblique left-lateral strike slip (with normal) mechanism (strike: 67°, dip: 68°, rake: − 28°).

We applied the grid search regional moment tensor inversion (RMT) method of Herrmann, (2013) to calculate the moment tensor. Specific details to perform the RMT inversion analysis, including Green's functions generation, waveform processing, grid search inversion and quality control of solution, can be found in the studies, such as Herrmann et al. (2011) and Herman et al. (2014), with application to the Chiang Rai, Thailand, earthquake sequence (Noisagool et al. 2016; Pananont et al. 2017).

We generated RMT inversions using waveforms, based on rotations defined both before and after re-alignment. Green's functions were developed from the one-dimensional velocity model of northern Thailand (Pananont et al. 2017). We used good-quality waveforms observed at 3 borehole stations: NANS, CRMM and CRMJ, which are at distances of 92, 135 and 180 km, respectively, from the source, with earthquake to station azimuths of 220°, 286° and 292°, respectively. For these stations there are very significant differences between the RMT determined using the final (correct) orientation and the initial TMD (metadata) orientation. We use the same parameters for the analyses before and after alignments in the RMT processing (time window between − 6 and 60 s of the signal with respect to the P pick), filtering the waveforms and Green's functions in the 0.03–0.10 Hz (33–10 s period range) and using the same distance weighting.

The Laos earthquake RMT solution before orientation correction does provide a good fit between observed and predicted waveforms in all components at the three stations (Fig. 4a), generating a best fitting focal mechanism at 7.0 km depth (Fig. 4b) with a magnitude Mw 6.1, and nodal plane strike, dip, and rake of 155°, 90°, and 10°, respectively (alternate plane: 65°, 80°, and 180°). These results, however, have a very large location error ~ 32 km (Fig. 4c) and a significantly different focal mechanism from the USGS solution. Also the transverse components at the CRMM and CRMJ stations require large time shifts of more than 9 s to achieve the waveform matching. The RMT result of this earthquake event, after correcting station orientations, has a similar best fit value, for depth and magnitude with the previous result (67% fit, 6.0 km depth and Mw 6.1) (Fig. 4e), but has a substantially different focal mechanism from the original (misoriented) model with a nodal plane strike, dip, and rake of 70°, 85°, and 5°, respectively (alternate plane: 340°, 85°, and 175°). This revised focal mechanism also agrees much better with the USGS W phase moment tensor. In this case, it can be seen that the waveform polarities of waveform before and after alignments (Fig. 4a and d), due to the sensor misorientation values 164°, 114° and 57° of NANS, CRMM and CRMJ station flip the event (on the preferred fault plane) from left-lateral to right-lateral strike slip.

We also examined the effect on the RMT for a local, smaller earthquake that occurred in Wang Nuea, Lampang, Thailand (19.249°N 99.617°E) on 2019-02-20 09:05:41, with a magnitude M_{Lv} 4.9, at 5 km depth (as reported by TMD). Buildings near the epicenter were slightly damaged. We selected two surface stations that were well oriented (LAMP and SUAB) and one borehole station (CMPR) with a large misorientation (in the TMD metadata) of 180°. In the RMT processing of this smaller event, we filtered the waveforms and Green's functions in the 0.04–0.10 Hz bandpass. The observed and predicted waveforms are fit 43% and 51% at 6 km depth with RMT strike, dip, rake of 175°, 65°, 169° (before) and 186°, 67°, − 153° (after) correction (Fig. 5a–d), that corresponds to a right-lateral strike slip fault on the southern part of Phayao fault zone. Because this is primarily a strike slip event, the ~ 180° misorientation of the CMPR station has only a slight effect on the focal mechanism solution. This is a result of the best fit balancing weighting of LAMP and SUAB stations and down weighting the large time shift of CMPR station in the waveform matching. However, the needed large shift of the origin time has the effect of producing a mislocation of up to 5.4 km from the true location (Fig. 5b).

In a test of how a sensor's misorientation can affect the time shift of observed and calculated waveforms and the resulting focal mechanism in the RMT analysis, done by using only radial and tangential components of LAMP station, we found that if the misorientation of the sensor is more than 10° from north, it will cause a time shift up

(See figure on next page.)

Fig. 4 The RMT solution of Laos earthquake after (**a**, **b**, **c**) and before (**d**, **e**, **f**) realignment using waveform data from 3 stations (NANS, CRMM and CRMJ) with azimuth from source of 225°, 295° and 289°, respectively. **a** and **d** A comparison of observed (red traces) and predicted (blue traces) vertical, radial, and transverse waveforms. **b** and **e** A representative of best fitting focal mechanism versus depth curve indicating the best fitting focal mechanism of 66% at 7.0 km depth and 67% at 6.0 km depth before and after alignments, respectively. **c** and **f** Estimate of source location error and time shifts for the inversion

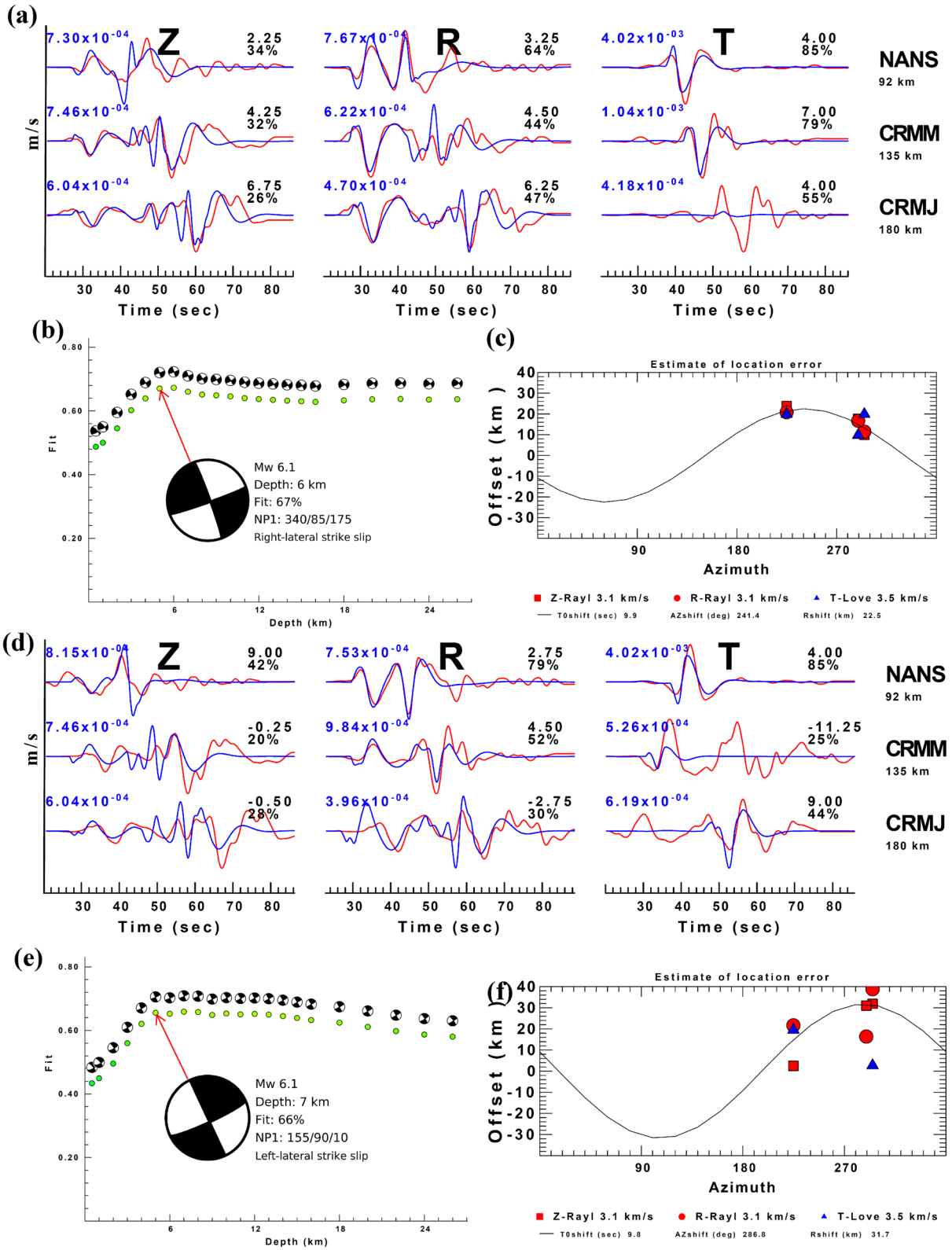

Fig. 4 (See legend on previous page.)

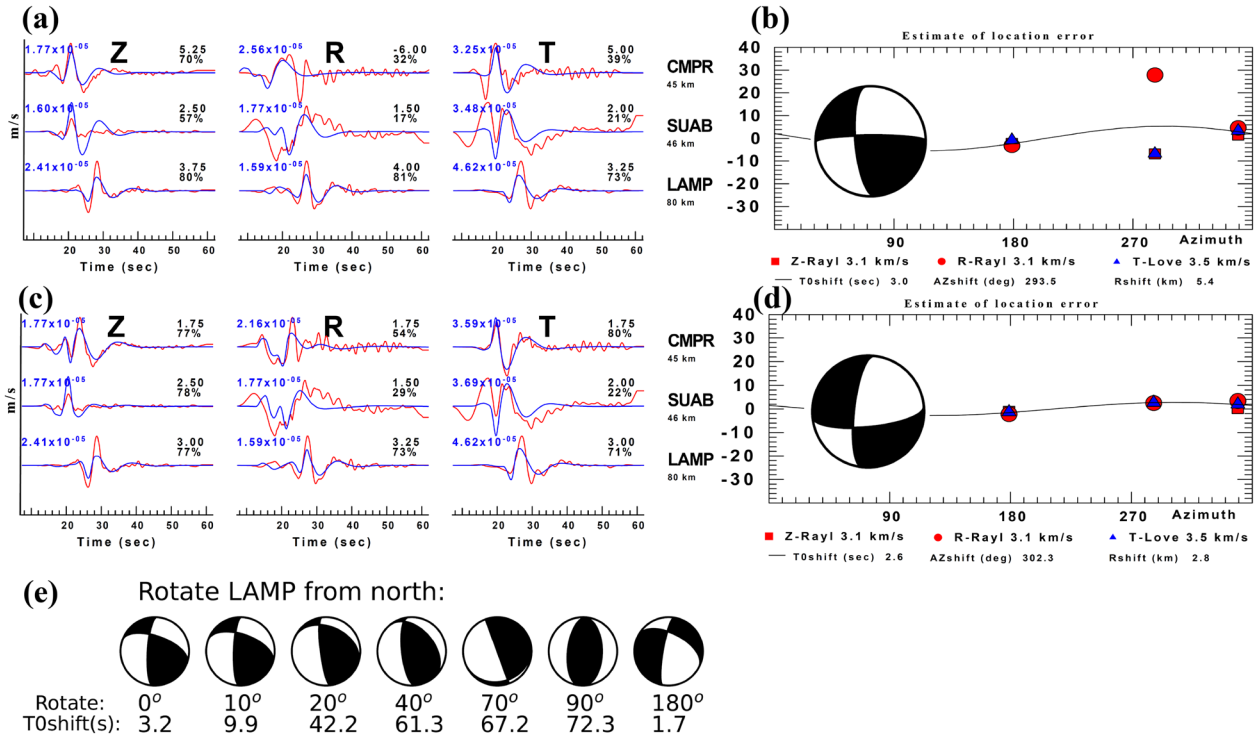

Fig. 5 The RMT waveform matching and focal mechanism and mislocation of the Wang Nuea earthquake before (**a**, **b**) and after (**c**, **d**) alignments using waveforms from 3 stations (CMPR, SUAB and LAMP) with azimuth from source of 287°, 349° and 179°, respectively. **e** The shift in origin time for waveform matching and focal mechanisms from RMT solutions as a result of rotation of LAMP station 0°–180° from north

to 10 s or mislocation up to 45 km. When, the sensor's misorientation is between 20 and 90°, the time shift is larger and we start to see the resulting focal mechanism changing from the correct sensor orientation (Fig. 5e).

Misorientation effects on receiver function stacking

To examine how sensor misorientation can influence receiver function models, we apply teleseismic receiver function analyses (Ammon et al. 1990) using three-component waveforms for teleseismic earthquakes. We isolate the radial receiver function by deconvolving the vertical component from radial (SV) and tangential (SH) components, then stacking the receiver functions by the bootstrap iteration slant stacking technique (Sandvol et al. 1998; Al-Damegh et al. 2005). We determine crustal thickness and the average Vp/Vs ratio of the crust beneath each seismic station.

Moderate misorientations of less than 20° have only a minor effect on the results of H-κ stacking (Zeng et al. 2020), however for larger misorientation the effects are significant. We estimated the crustal thickness and the Vp/Vs ratio of the crust beneath the CRMM station, which had a difference in orientation before and after correction of 112°. We slant stacked 31 radial receiver functions detected from teleseismic earthquakes with magnitudes larger than 6.5 and epicentral distance range of 25–95 degrees from the CRMM station during 2018 to 2020 with good azimuthal coverage. We weighted the Ps, PPs and PSs at 0.40, 0.30 and 0.05, respectively, and completed 100 bootstrap iterations. We used the same parameters for waveform analysis in both the before and after orientation correction analyses. In our analysis of the waveforms before re-orientation, we observed that the radial receiver function was inverted for all converted phases especially direct P and Ps, and converted phases cannot be clearly identified and are incoherent on each trace. These pre-correction models produced Moho depths and Vp/Vs ratio distributed in the range 36–43 km (with some scattering in Moho depth of up to 50 km) and high Vp/Vs ratio between 1.8 and 1.9 (Fig. 6a). When we correct the sensor orientation for this station, the results show a correctly oriented receiver function and coherent and clear arrivals of direct P, Ps and multiples. We obtain a 32.6-km depth for the Moho and a Vp/Vs of 1.74 with an uncertainty of ± 1.16 km and ± 0.025, respectively, derived from the standard deviation of the 100 bootstrap results (Fig. 6b). We also estimated the crustal properties beneath the CRAI station using the corrected orientation results and obtained a crustal thickness of 29.0 ± 2.6 km and a Vp/Vs of 1.79 ± 0.095 (Additional file 1: Fig. S5)

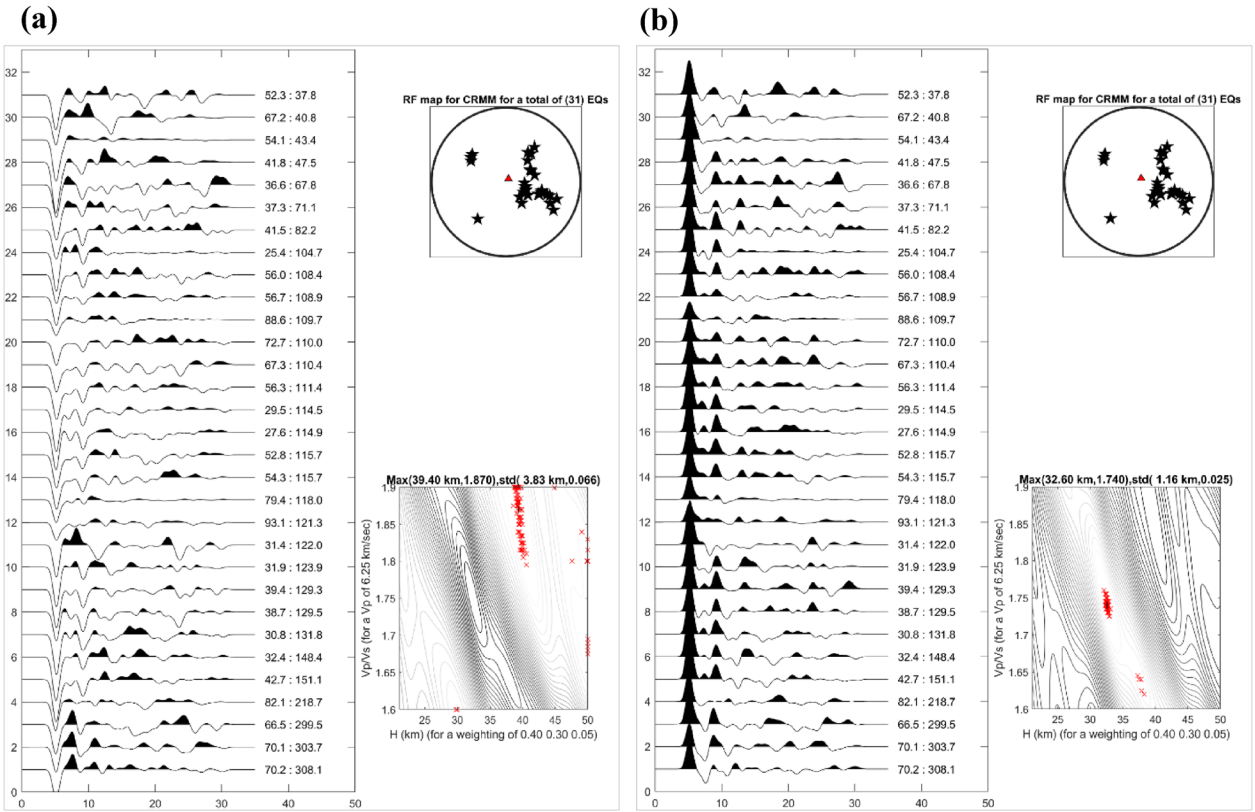

Fig. 6 31 stacked radial receiver functions and Moho depth vs Vp/Vs plot beneath CRMM station from teleseismic earthquake. **a** Polarity reversal of receiver function before correcting orientation, and unstable of Moho depth vs Vp/Vs results and **b** stacked results after correcting orientation, show clear peak of P and Ps resulting in stable Moho depth and Vp/Vs

comparable to the results from the study of Yu et al. (2017).

In order to better understand the effect of the amount of sensor misorientation on the resulting receiver function, we applied different sensor orientations for the CRMM station, varied by 30° increments from 0° (true north) to 180° (south). We then recalculated radial receiver functions by using the M 6.4 Northern Mariana Islands earthquake of 2019-06-28 (azimuth of 71° and distance of 37° from the CRMM station). A plot of radial receiver functions for each sensor misorientation is shown in Fig. 7. At 0° sensor's misorientation (presumed correct sensor's orientation), the receiver function was clear, especially for the P and Ps converted phases. When the sensor's misorientation is 30° from north, the receiver function is still almost the same but the direct P phase's maximum amplitude decreases from 0.29 to 0.22 (25% decrease) which corresponds to effects seen by Wang et al. (2016) of the misorientation on P-wave amplitude. When the sensor's misorientation is 60°, the direct P phase's maximum amplitude decrease to 0.12 (60% decrease). When the sensor's misorientation is 90° (the apparent radial component becomes the apparent transverse component), the amplitude of P phase is strongly diminished. When a sensor's misorientation is more than 90° (120°, 150° and 180°), the radial receiver function reverses (i.e., the P phase amplitude has a 180° phase shift to those of the 0° sensor's misorientation as shown in Fig. 7).

Conclusions

We applied a P-wave polarization methodology to estimate the sensor misorientation for the TMD seismic network, using both regional and teleseismic earthquakes. For the 45 surface stations, over the time period of 2009–2022 (depending on the time of installation or replacement of equipment), 37 stations were misoriented by 0–15° from true north, 8 stations have a larger misorientation of the sensors of more than 15°. Some stations have temporal changes in sensor orientation when TMD upgraded the stations. For 26 borehole stations, we found seismometers were oriented differently than reported in the original metadata. For the short-period borehole stations there was an ~ 180° reversal of polarity, as a result of significant differences in the instrument response for the short period and broad band instruments (Additional

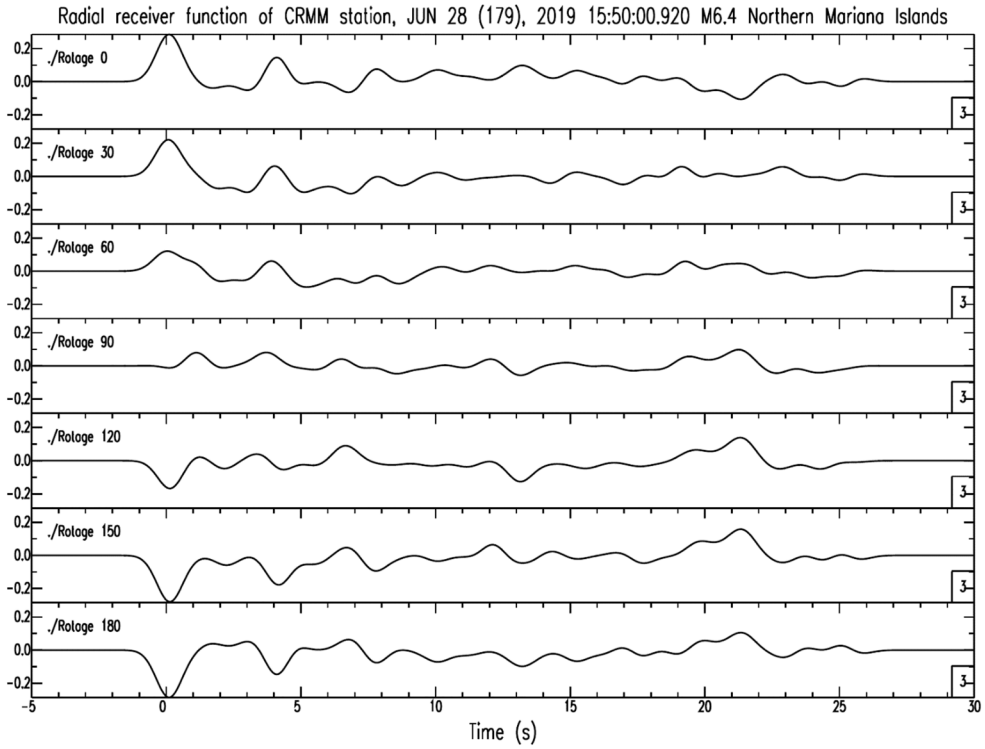

Fig. 7 Plot of radial receiver functions beneath CRMM station for sensor rotation 0°, 30°, 60°, 90°, 120°, 150° and 180° from north from top to bottom, respectively. (0° means correct orientation.)

file 1: Fig. S3). We found that the instrument misorientations can have a significant influence on standard seismological studies. The misorientation effects for regional moment tensor solutions show that a large misorientation can flip the focal mechanism results. We have found that some receiver function analysis results and moment tensor inversion models using the original station metadata were incorrect as a result of errors in that original metadata, especially for borehole stations. When sensor misalignment exceeds 10°, it can cause large relative time shifts and mislocation in RMT process, and misorientations > 20° can significantly affect receiver function waveforms and the determined Moho depth and Vp/Vs ratio results. We also investigated what potentially caused the erroneous relative orientations using the ambient noise correlation method, which TMD uses to determine the orientation of borehole stations. We found that the difference in PSD of ground motion of ~ 10–20 dB makes the orientation results differ by only ~ 3°. We, however, found that differences in instrument response between the reference and test sensors can cause a much larger misorientation. Finally, the sensor orientation results in this study provide a reference correction for the TMD seismic network managers and a suggestion to other seismic networks on how to avoid similar errors that may lead to sensor misorientations in future deployments. Data users can access up-to-date correct orientations and information of these stations from the TMD official website (https://earthquake.tmd.go.th/stations.html) to correct or validate their results and for future seismological studies.

Supplementary Information

The online version contains supplementary material available at https://doi.org/10.1186/s40562-023-00278-7.

Additional file 1: Table S1 Seismometer orientation result and station details, including earthquake events using in analysis of 45 surface stations. **Table S2** Seismometer orientation result and station details of 26 borehole stations. **Fig. S1** Signal correlation between the surface referenceand down-hole sensorwhich has the same instrument response and orientation results. **a** and **d** Time series of reference sensorand a borehole sensorin perfect N/S orientation and signal differrence plot for day and night times, respectively. **b** and **e** The peak of the coherence curve therefore corresponds to the angle of rotation which best matched the reference sensorand the overall amplitude similarity of the borehole rotated signalfor day and night times, respectively. **c** and **f** A plot of coherence, frequency and rotation angle for day and night times, respectively, the black line curve show the frequency use in correlation calculation. **Fig. S2** Signal corelation between the surface referenceand down-hole sensor**a** show the down-hole test sensor aligned at ~178° or polarity reversal **b** caused by the difference instrument response of the surface reference sensor. **Fig. S3** The phase response plot of a Guralp CMG-3ESPCand CMG-3TB. **Fig. S4** Transverse and radial component of the RATC station of the M 6.5 Taiwan earthquake occurring on 17 September 2022. The correct orientation

shows very small P-Wave energy on the transverse componentcompared to that of radial component.. **Fig. S5** Radial receiver functions and Moho depth vs Vp/Vs plot beneath CRAI station from 27 teleseismic earthquakes.

Acknowledgements
We acknowledge the Thai meteorological department (TMD) for supporting this research and greatly appreciate the editors and anonymous reviewers for their constructive comments.

Author contributions
PP_1(Pornsopin) performed the analysis and wrote the manuscript. All authors discussed the interpretation of the data processing result. PP_1, PP_2(Pananont), KPF and ES contributed to the writing and revisions. All authors read and approved the final manuscript.

Funding
Not applicable.

Availability of data and materials
Seismic data and metadata used in this study are available for author and agreed by the Earthquake observation division, Thai Meteorological Department. The Python code (OrientPy toolbox) to evaluate the sensor misorientation from P-wave polarization was developed by Pascal Audet [(Braunmiller et al. 2020); https://github.com/nfsi-canada/OrientPy]. Some of the figures were prepared using the Generic Mapping Tools version 6.0 (Wessel et al. 2019). Regional moment tensor inversion (RMT) code using Computer Programs in Seismology version 3.30 [(Herrmann 2013); http://www.eas.slu.edu/eqc/eqccps.html]. The MATLAB code to slant stack the receiver functions was provided by Eric Sandvol and data were analyzed with the Seismic Analysis Code: SAC (Goldstein et al. 2003). Determination of relative orientation of a borehole sensor relative to a surface reference sensor using Scream! Version 4.6 provided by Güralp Systems Ltd.

Declarations

Competing interests
The authors declare that they have no competing interests.

Received: 9 September 2022 Accepted: 30 April 2023
Published online: 22 May 2023

References

Al-Damegh K, Sandvol E, Barazangi M (2005) Crustal structure of the Arabian plate: new constraints from the analysis of teleseismic receiver functions. Earth Planet Sci Lett 231(3):177–196. https://doi.org/10.1016/j.epsl.2004.12.020

Ammon CJ, Randall GE, Zandt G (1990) On the nonuniqueness of receiver function inversions. J Geophys Res Solid Earth 95(B10):15303–15318. https://doi.org/10.1029/JB095iB10p15303

Braunmiller J, Nabelek J, Ghods A (2020) Sensor orientation of Iranian broadband seismic stations from P-Wave particle motion. Seismol Res Lett 91(3):1660–1671. https://doi.org/10.1785/0220200019

Burch RF, Atomic Weapons Research Establishment (Great Britain) (1993) A three-component borehole seismometer system: development and operation. In: Atomic Weapons Research Establishment

Büyükakpınar P, Aktar M, Maria Petersen G, Köseoğlu A (2021) Orientations of broadband stations of the KOERI seismic network (Turkey) from two independent methods: P- and Rayleigh-Wave polarization. Seismol Res Lett 92(3):1512–1521. https://doi.org/10.1785/0220200362

Doran AK, Laske G (2017) Ocean-bottom seismometer instrument orientations via automated Rayleigh-wave arrival-angle measurements. Bull Seismol Soc Am 107(2):691–708. https://doi.org/10.1785/0120160165

Ensing JX, van Wijk K (2018) Estimating the orientation of borehole seismometers from ambient seismic noise. Bull Seismol Soc Am 109(1):424–432. https://doi.org/10.1785/0120180118

Goldstein P, Dodge D, Firpo M, Minner L (2003) 85.5 SAC2000: signal processing and analysis tools for seismologists and engineers. Int Geophys 81:1613–1614. https://doi.org/10.1016/S0074-6142(03)80284-X

Herman MW, Herrmann RB, Benz HM, Furlong KP (2014) Using regional moment tensors to constrain the kinematics and stress evolution of the 2010–2013 Canterbury earthquake sequence, South Island, New Zealand. Tectonophysics 633:1–15. https://doi.org/10.1016/j.tecto.2014.06.019

Herrmann R (2013) Computer programs in seismology: an evolving tool for instruction and research. Seismol Res Lett 84:1081–1088

Herrmann RB, Malagnini L, Munafo I (2011) Regional moment tensors of the 2009 L'Aquila earthquake sequence. Bull Seismol Soc Am 101(3):975–993. https://doi.org/10.1785/0120100184

Niu F, Li J (2011) Component azimuths of the CEArray stations estimated from P-wave particle motion. Earthq Sci 24(1):3–13. https://doi.org/10.1007/s11589-011-0764-8

Noisagool S, Boonchaisuk S, Pornsopin P, Siripunvaraporn W (2016) The regional moment tensor of the 5 May 2014 Chiang Rai earthquake (Mw = 6.5), Northern Thailand, with its aftershocks and its implication to the stress and the instability of the Phayao Fault Zone. J Asian Earth Sci 127:231–245. https://doi.org/10.1016/j.jseaes.2016.06.008

Ojo AO, Zhao L, Wang X (2019) Estimations of sensor misorientation for broadband seismic stations in and around Africa. Seismol Res Lett 90(6):2188–2204. https://doi.org/10.1785/0220190103

Pananont P, Herman MW, Pornsopin P, Furlong KP, Habangkaem S, Waldhauser F, Wechbunthung B (2017) Seismotectonics of the 2014 Chiang Rai, Thailand, earthquake sequence. J Geophys Res Solid Earth 122(8):6367–6388. https://doi.org/10.1002/2017jb014085

Ringler AT, Hutt CR, Persefield K, Gee LS (2013) Seismic station installation orientation errors at ANSS and IRIS/USGS stations. Seismol Res Lett 84(6):926–931. https://doi.org/10.1785/0220130072

Sandvol E, Seber D, Calvert A, Barazangi M (1998) Grid search modeling of receiver functions: Implications for crustal structure in the Middle East and North Africa. J Geophys Res 103:26899–26917. https://doi.org/10.1029/98JB02238

Scholz J-R, Barruol G, Fontaine FR, Sigloch K, Crawford WC, Deen M (2017) Orienting ocean-bottom seismometers from P-wave and Rayleigh wave polarizations. Geophys J Int 208(3):1277–1289. https://doi.org/10.1093/gji/ggw426

Vecsey L, Plomerová J, Jedlička P, Munzarová H, Babuška V (2017) Data quality control and tools in passive seismic experiments exemplified on the Czech broadband seismic pool MOBNET in the AlpArray collaborative project. Geosci Instrum Method Data Syst 6(2):505–521. https://doi.org/10.5194/gi-6-505-2017

Wang X, Chen QF, Li J, Wei S (2016) Seismic sensor misorientation measurement using P-Wave particle motion: an application to the NECsaids array. Seismol Res Lett 87(4):901–911. https://doi.org/10.1785/0220160005

Weglarczyk S (2018) Kernel density estimation and its application. ITM Web of Conf 23:00037. https://doi.org/10.1051/itmconf/20182300037

Wessel P, Luis JF, Uieda L, Scharroo R, Wobbe F, Smith WHF, Tian D (2019) The generic mapping tools version 6. Geochem Geophys Geosyst 20(11):5556–5564. https://doi.org/10.1029/2019GC008515

Yu Y, Hung TD, Yang T, Xue M, Liu KH, Gao SS (2017) Lateral variations of crustal structure beneath the Indochina Peninsula. Tectonophysics 712–713:193–199. https://doi.org/10.1016/j.tecto.2017.05.023

Zeng S, Zheng Y, Niu F, Ai S (2020) Measurements of seismometer orientation of the first phase CHINArray and their implications on vector-recording-based seismic studies. Bull Seismol Soc Am 111(1):36–49. https://doi.org/10.1785/0120200129

Publisher's Note